

Use of *In Situ* and Airborne Multiangle Data to Assess MODIS- and Landsat-Based Estimates of Directional Reflectance and Albedo

Miguel O. Román, *Member, IEEE*, Charles K. Gatebe, Yanmin Shuai, Zhusen Wang, Feng Gao, Jeffrey G. Masek, Tao He, Shunlin Liang, *Senior Member, IEEE*, and Crystal B. Schaaf, *Member, IEEE*

Abstract—The quantification of uncertainty in satellite-derived global surface albedo products is a critical aspect in producing complete, physically consistent, and decadal land property data records for studying ecosystem change. A challenge in validating albedo measurements acquired from space is the ability to overcome the spatial scaling errors that can produce disagreements between satellite and field-measured values. Here, we present the results from an accuracy assessment of MODIS and Landsat-TM albedo retrievals, based on collocated comparisons with tower and airborne Cloud Absorption Radiometer (CAR) measurements collected during the 2007 Cloud and Land Surface Interaction Campaign (CLASIC). The initial focus was on evaluating inter-sensor consistency through comparisons of intrinsic bidirectional reflectance estimates. Local and regional assessments were then performed to obtain estimates of the resulting scaling uncertainties, and to establish the accuracy of albedo reconstructions during extended periods of precipitation. In general, the satellite-derived estimates met the accuracy requirements established for the high-quality MODIS operational albedos at 500 m (the greater of 0.02 units or $\pm 10\%$ of surface measured values). However, results reveal a high degree of variability in the root-mean-square error (RMSE) and bias of MODIS visible (0.3–0.7 μm) and

Landsat-TM shortwave (0.3–5.0 μm) albedos; where, in some cases, retrieval uncertainties were found to be in excess of 15%. Results suggest that an overall improvement in MODIS shortwave albedo retrieval accuracy of 7.8%, based on comparisons between MODIS and CAR albedos, resulted from the removal of sub-grid scale mismatch errors when directly scaling-up the tower measurements to the MODIS satellite footprint.

Index Terms—Biosphere, ecosystems, land surface, remote sensing.

I. BACKGROUND

THE quantification of uncertainty in global surface albedo products from both MODIS and Landsat satellites is a critical part of producing complete, physically consistent, global, and decadal land property data records. The MODIS-BRDF/albedo standard product, available globally since 2000 at resolutions from 0.5 to 5 km, has been validated to Committee on Earth Observation Satellites (CEOS) Stage 3 (i.e., over a widely distributed set of locations and time periods via several ground-truth and validation efforts) [1]. This validation stage is a pre-requisite for any data product that is used for monitoring change over time [2]. The high-quality primary algorithm for the MODIS standard albedo product (MCD43) has also been shown to produce consistent global quantities over a variety of land surface types and snow-covered conditions [3]–[9]. On the other hand, the combined MODIS/Landsat albedo product (hereby termed “Landsat albedo”), which is based on per-class MODIS BRDF shapes based on uniform land cover characteristics, has been shown to provide a more detailed landscape texture and achieve good agreement with in situ data over a limited number of field stations [10]. Additional assessments over a wide range of spatial (from 10 s of meters to 5–30 km) and temporal scales (from daily to monthly) are nonetheless required to accurately provide end users with a pixel-specific measure of product accuracy—both in terms of retrieval quality (e.g., given a limited number of cloud-free satellite observations) and their ability to capture albedo trends under conditions of seasonal or rapid surface change.

A continuing challenge in validating satellite albedo retrievals is the ability to overcome the spatial scaling errors that contribute to disagreements between satellite and field-measured values [4]–[6], [8]. Recent studies have acquired measurements atop tall (> 400 m) towers to properly “scale-up” to satellite measurements [7], [11]. Other efforts have used high

Manuscript received January 30, 2013; revised September 24, 2012 and January 4, 2013; accepted January 15, 2013. This work was supported by the Science Mission Directorate of the National Aeronautics and Space Administration as part of the Earth Observing System, Radiation Sciences Program, the Terrestrial Ecology Program, and the Airborne Sciences Program. The work of C. K. Gatebe was supported by NASA Grant NNX08AF89G. The work of C. B. Schaaf was supported by NASA Grant NNX12AL38G and U.S. Department of Energy (DOE) Atmospheric Radiation Measurement (ARM) Program under Grant DOE-DE-FG02-06ER64178.

M. O. Román and J. G. Masek are with the NASA Goddard Space Flight Center, Greenbelt, MD 20771 USA (e-mail: Miguel.O.Roman@nasa.gov; jeffrey.g.masek@nasa.gov).

C. K. Gatebe is with the NASA Goddard Space Flight Center, Greenbelt, MD 20771 USA and also with the Universities Space Research Association (USRA), Columbia, MD 21044 USA (e-mail: charles.k.gatebe@nasa.gov).

Y. Shuai is with the NASA Goddard Space Flight Center, Greenbelt, MD 20771 USA and also with Earth Resources Technology Inc., Laurel, MD 20707 USA (e-mail: Yanmin.Shuai@ertcorp.com).

Z. Wang and C. B. Schaaf are with the Department of Environmental, Earth and Ocean Sciences, University of Massachusetts, Boston, MA 02125 USA and also with the Center for Remote Sensing, Department of Geography and Environment, Boston University, Boston, MA 02215 USA (e-mail: wangzhs@bu.edu; schaaf@bu.edu).

F. Gao is with the USDA-ARS Hydrology and Remote Sensing Laboratory, Beltsville, MD 20705, USA (e-mail: Feng.Gao@ars.usda.gov).

T. He and S. Liang are with the Department of Geographical Sciences, University of Maryland, College Park, MD 20742, USA (e-mail: the@umd.edu; sliang@umd.edu).

Color versions of one or more of the figures in this paper are available online at <http://ieeexplore.ieee.org>.

Digital Object Identifier 10.1109/TGRS.2013.2243457

resolution imagery to consider the spatial representativeness of the tower observation footprint to the MODIS pixel [7], [12]. While these methods provide a way to identify locations where direct “point-to-pixel” assessments can be performed with high confidence; they present their own set challenges (e.g., in the United States, instruments atop tall towers cannot be left operating year-round, due to heavy icing and bad weather). Accordingly, the major question surrounding this effort is: how can the accuracy of satellite-derived albedos be quantified over regions where “point-to-pixel” assessments cannot be performed with high confidence?

In this effort, we present the results from an assessment of MODIS and Landsat-TM albedo retrievals based on collocated comparisons with tower and airborne measurements obtained during the 2007 Cloud and Land Surface Interaction Campaign (CLASIC’07) [13], [14] over the Atmospheric Radiation Measurement (ARM) facility at the Southern Great Plains (SGP) site in OK [15]; also known as the ARM Cloud and Radiation Testbed (ARM/CART). For the airborne data sets, we have employed the retrieval scheme presented in [16], which follows the operational sequence used to retrieve the MODIS surface reflectance and BRDF/albedo [17], [18], based on high-quality multiangular reflectance measurements obtained by NASA’s Cloud Absorption Radiometer (CAR) [19], [20].

This paper is structured as follows. In Section II, we briefly review the albedo retrieval techniques used by the MODIS, Landsat, and CAR instruments (Section II-A); assess the calibration performance of the CAR spectral channels during the period of CLASIC’07 (Section II-B); describe the set of intrinsic narrowband-to-broadband spectral albedo coefficients for CAR retrievals (Section II-C); illustrate the individual BRDF retrieval and albedo reconstruction periods for the CLASIC’07 experiment (Section II-D); and provide a comparison of at-ground reflectances between the CAR, Landsat-TM, and MODIS data (Section II-E). Readers are referred to [16] for detailed descriptions of the CLASIC’07 experiment (including retrieval of CAR and MODIS BRDF/albedo data sets); and [10] for a complete description of the Landsat albedo retrieval strategy. The remainder of this paper is organized into three main sections. Section III examines the diurnal performance of broadband albedos derived from CAR, MODIS, and Landsat-TM based on comparisons against available tower-based albedo measurements. In Section IV, using the fine-resolution airborne CAR measurements, we then quantify the pixel-specific accuracy of MODIS and Landsat-TM retrievals over a mixture of landscapes extending beyond the tower observation footprint at the ARM/CART site. Section V concludes with a summary of the study and provides suggestions for future research.

II. RETRIEVAL STRATEGY

A. Instantaneous Albedos From CAR, MODIS, and Landsat

The CAR, MODIS, and Landsat albedo retrieval schemes employ the kernel model parameters from the reciprocal version of the semi empirical Ross Thick-LiS parse linear BRDF model (RTLSR) [21]–[23]. The algorithms use the RTLSR kernel weights to compute intrinsic surface albedos (i.e., black sky

albedo for direct beam at local solar noon and white sky albedo for isotropic diffuse radiation) [24], [25]. To accurately compare these intrinsic quantities against ground-based albedos, the black-sky and white-sky albedos must then be combined as a function of solar geometry and atmospheric state to compute instantaneous albedo under assumptions of isotropic diffuse illumination [21], [26]. The BRDF shape derived from clear-sky observations can then be used to derive albedo values in all sky conditions [5]. Most recently, the computation of MODIS instantaneous albedos was updated to account for the effects of multiple scattering and anisotropic diffuse illumination [6]. Intrinsic albedo quantities derived from RTLSR BRDF model inversions can then be combined and screened with in situ estimates of cloud fraction (< 0.6), 550 nm aerosol optical depth (AOD), solar zenith angle (SZA), and the proportion of downwelling diffuse illumination to compute clear-sky instantaneous albedos.

B. CAR Instrument Performance During CLASIC’07

During the CLASIC’07 experiment, radiometric calibration of the CAR spectral channels was made at the NASA Goddard Space Flight Center Radiometric Calibration Facility (GSFC-RCF) [27]. A description of the calibration scheme, using a series of integrating spheres with diameters of 1.83 m, 1.22 m, and 0.51 m, covering all of the CAR’s spectral channels, can be found in [28]. The conversion from Digital Numbers (DNs) to Level 1 at-sensor radiances is determined from the instrument’s response for at least two known radiance levels and then determining the instrument gain (slope) and offset (intercept) for each wavelength across the sensor band pass. The estimated errors associated with this radiometric conversion vary from $\pm 1\%$ to $\pm 3\%$ for all spectral channels [19], [28]. Radiometric calibration was performed prior to and after the CLASIC’07 experiment. In the past, to determine a suitable calibration for a given flight during the experiment, a linear change between the preflight and post flight calibration was assumed as a function of only the number of flights flown during an entire campaign. For the CLASIC’07 experiment, however, both the pre- and post-calibration coefficients were averaged. This was found to be representative of each flight scenario, and made it easier to account for uncertainties related to calibration, stability, and wavelength errors. We note that the calibration ratios, post flight-to-preflight, varied between 0.9691 (at $\Lambda = 0.472 \mu\text{m}$) and 1.1845 (at $\Lambda = 0.340 \mu\text{m}$).

C. Narrowband to Broadband Conversion of Intrinsic Albedos

Since field-measured albedos are commonly measured as broadband quantities, an equivalent set of broadband albedos can be generated for the Visible (0.3–0.7 μm), NIR (0.7–5.0 μm), and the entire spectrum of solar radiation ([SW] 0.3–5.0 μm), based on empirical relations between ground-based albedo measurements and satellite observations [30]. CAR narrowband-to-broadband spectral albedo coefficients were also generated for each spectral channel by determining the downward fluxes (i.e., direct and diffuse) using a library of

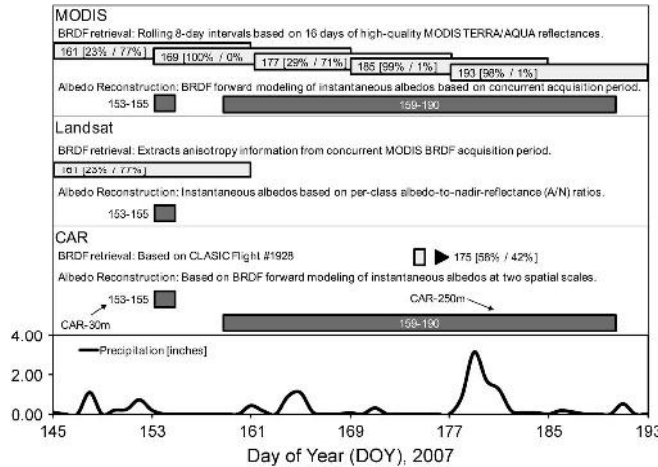


Fig. 1. Surface BRDF retrievals (light gray bars) and instantaneous albedo reconstruction periods (dark-gray bars) obtained during CLASIC'07 (DOY 137–193, 2007) for MODIS, Landsat-TM, and CAR. For each BRDF retrieval period, the numbers inside the bars illustrate the DOY followed by the percentage of best quality (original, full inversion) and gap-filled values: DOY [%Full-Inversion/%Gap Filled].

30 reflectance spectra of representative land covers in the ARM Southern Great Plains (SGP) region [29]

$$\alpha_{\text{short}} = 0.3922\alpha_3 + 0.2663\alpha_4 + 0.2701\alpha_5 + 0.1668\alpha_7 \quad (1)$$

$$\alpha_{\text{vis}} = 0.6919\alpha_3 + 0.3106\alpha_4 + 0.0375\alpha_5 + 0.0314\alpha_7 \quad (2)$$

$$\alpha_{\text{nir}} = 0.2256\alpha_3 + 0.2046\alpha_4 + 0.4235\alpha_5 + 0.2915\alpha_7. \quad (3)$$

The CAR upward fluxes were directly obtained from the library of SGP reflectance spectra; while the downward fluxes were obtained by performing multiple MODTRAN 5.1 runs [31] for a broad range of snow-free conditions (21 atmospheric visibility values for different aerosol loadings, 2 atmospheric profiles, and solar zenith angles ranging from 0° – 80° with the increment of 1°). As with the MODIS and Landsat coefficients, multiple narrowband channel combinations were tested to determine the albedo coefficients that resulted in the smallest residual standard error (RSE). Since the estimation of variances associated with CAR channels 1, 2, and 6 coefficients was too large, these channels were simply dropped.

D. BRDF/Albedo Retrieval Scenarios During CLASIC'07

Fig. 1 provides a summary of the individual BRDF retrieval and albedo reconstruction periods for CAR, MODIS, and Landsat-TM collocated with daily estimates of precipitation obtained from ground-based stations. Note that the retrieval scenarios varied by sensor. For instance, Landsat-TM albedos were reconstructed in 15 min intervals for Day of the year, DOY 153–155. This short time period was chosen to better represent the per-class albedo-to-nadir-reflectance (A/N) ratios derived from the concurrent MODIS acquisition period (DOY 161). The CAR surface BRDF retrievals were based on a single date of acquisition (DOY 175), while the MODIS BRDF results were based on rolling 8-day intervals from all clear-sky, high quality, atmospherically-corrected surface reflectances available during a 16-day period.

The CAR and MODIS instantaneous albedos were derived from BRDF forward modeling, representing the solar geometry and specific ratio of direct to diffuse illumination [32]. For all cases, instances of cloud contamination (Cloud Fraction > 0.6) and large solar zenith angles $> 70^\circ$ were excluded. CAR-derived albedos were further partitioned into two different spatial grid scales: 1) a medium resolution mode (CAR-30 m) to match the scale of Landsat-TM data during the period of DOY 153–155; and 2) a coarse resolution mode (CAR-250 m) to match the scale of MODIS data during the period of DOY 159–190. The two modes were created to reduce the uncertainties resulting from spatial aggregation of the RTLSR-BRDF model parameters, which can lead to errors on the order of 6.5% in the predicted spectral bidirectional reflectance factors (BRF) [16].

For the period surrounding the Landsat-TM date of acquisition (DOY 154), 77% of the MODIS retrievals were based on high-quality “majority” full inversion values. Other BRDF retrieval periods were impacted by extended rainfall patterns. This resulted in either gaps in the measurements (DOY 166, 169, and 178–181), or in the majority of MODIS albedo reconstructions to be based on gap-filled BRDF values (DOY 160–161, 170–177). The latter relies on spatial and temporal fitting techniques to provide an estimate of the surface reflectance anisotropy (BRDF) for situations under cloud-contaminated conditions [33]. Note that MODIS gap-filled BRDF/albedo values are meant to provide a close, but not exact, representation of the underlying surface conditions; and should thus be interpreted with caution.

Unlike the MODIS gap-filled BRDF retrieval strategy, the gap-filling approach applied to CAR airborne data uses a different processing method. Instead of applying spatial/temporal fits, the scheme reutilizes the high-quality BRDF retrievals (observations ≥ 7) obtained during the same flight period (DOY 175) to process those areas where a full retrieval could not be made. An ancillary database derived from the co-located surface BRDF data ($\text{RSME} < 2\%$) is then parameterized with area-based proportions of land cover type to obtain a set of archetypal BRDF shapes. By assuming that surface BRFs scale linearly in a spatial sense [34], a full range of mixed BRDF patterns can be reconstructed. Since the gap-filled values from CAR are based on temporally collocated BRDF shapes, they should in principle be more temporally representative of the underlying surface conditions than their multi-date MODIS counterparts (albeit for a period of ± 16 days). For an in-depth look at the MODIS and CAR BRDF retrieval strategies, readers are referred to Section III in [16], where quality assurance (QA) summaries based on data from CLASIC'07 Flight #1928 are available.

E. Intercomparison of Spectral BRF Values

The daily albedo values retrieved from CAR, Landsat-TM, and MODIS data are impacted by varying degrees of uncertainty, including: 1) uncertainties in the BRDF and broadband albedo retrieval process (which depend on the number, angular distribution, and quality of the observations), uncertainties in the surface reflectance product (e.g., due to correction for

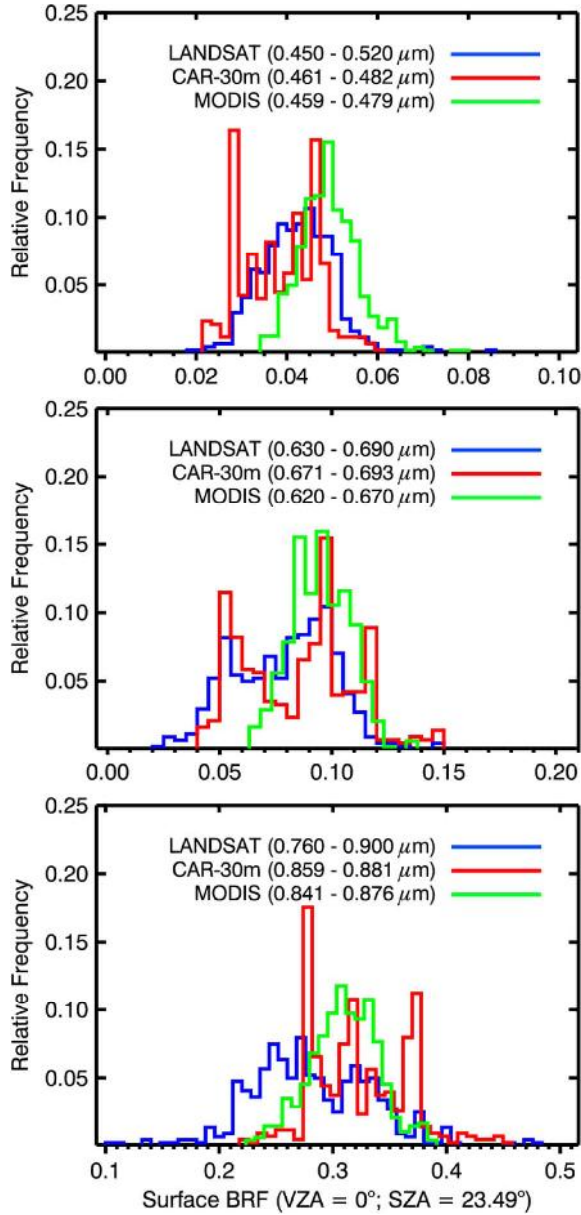


Fig. 2. Distribution of surface BRF values derived from CAR-30 m, MODIS, and Landsat-TM for three spectral regions (blue—top, red—center, and NIR—bottom) over the CLASIC'07 study area. For MODIS and CAR, the retrieved RTLSR-BRDF model parameters were applied in forward mode to predict the BRF values obtained by Landsat-TM at overpass time (DOY 154; VZA = 0°; SZA = 23.49°).

atmospheric and environmental effects, e.g., high-aerosol, missing or cloud-contaminated pixels); and 2) uncertainties due to scaling effects and georegistration inaccuracies. In this section, an intercomparison of intrinsic spectral BRF values was performed to reduce the number of uncertainties associated to the retrieval of instantaneous (or apparent) albedos, and simplify the assessment to that of an inherent optical property [25], [35]. This allowed us to further help constrain the assumption of temporal stability concerning the CAR Flight #1928 BRDF retrieval period (DOY 175, 2007), which fell outside of the Landsat-TM (DOY 153–155) albedo reconstruction period.

The histograms in Fig. 2 show the variations in the mean BRFs derived from CAR-30 m, Landsat-TM, and MODIS data, at the upscaled MODIS scale (500 m), for three spectral regions

(blue, red, and NIR) over the entire CLASIC'07 study domain (10 km × 10 km centered on the CART site). A statistical summary of the results (Table I) shows that the predicted BRF values from CAR-30 m remained within 2.26%, 0.97%, and 5.74% of the Landsat-TM results in the blue, red, and NIR spectral regions, respectively. It should also be noted that the CLASIC'07 study domain experienced an extended rainfall event prior to Landsat-TM overpass of DOY 154 (total rainfall = 1.37 inches). This resulted in a minor underestimation of the Landsat-TM BRF values obtained at overpass time; particularly in the NIR region, where soil conditions at plot-level scales (< 90 m) vary more rapidly under rainfall influence [36].

The differences in the at-ground NIR reflectances may have also been caused by random errors due to a slight overcorrection in the reflectance retrieval, or small differences in the relative spectral responses (RSRs) of each sensor (Fig. 3). To address the latter, an assessment of the CAR, MODIS, and Landsat-TM RSRs was performed using a library of 30 reflectance spectra obtained at the ARM/CART. Results confirm that the at-ground BRF reflectances remained below a ±2.0% threshold in the blue and NIR regions and ±4.9% in the red. The latter resulted from slight differences in the spectral bandpasses of CAR (870 nm) and MODIS (858 nm). Results were within the margin of error expected for satellite-derived reflectance values (the greater of 0.5% absolute reflectance or 5% of the recorded reflectance value) [52]. Thus, absent other downstream sources of measurement error, the CAR, MODIS, and Landsat-TM albedo values can be appropriately scaled and compared against each other.

III. LOCAL ASSESSMENT

A. Ground Measurements

We now examine the diurnal performance of broadband albedos derived from CAR, MODIS, and Landsat-TM based on comparisons against available tower-based albedo measurements acquired during CLASIC'07. Surface conditions at the ARM/CART were defined by a patchwork of mixed crops (both broadleaf and cereal), bare soils exposed by recent harvesting, small mixtures of trees and shrubs, as well as a few buildings and the occasional paved roads [35]. Measurements from a downward-facing pyranometer installed on a 60-m radiation tower at the ARM/CART site collected albedo and radiation fluxes in the shortwave (SW) (0.3–2.8 μm) waveband. Two additional instruments, a normal incidence pyrheliometer mounted on an automatic sun tracker and a shaded pyranometer riding on top of the sun tracker, measured direct and diffuse solar radiation incident upon the field station. Estimates of precipitation, cloud fraction, and aerosol optical depth, the latter two as viewed from a skyward-looking pyranometer and an AERONET sun photometer [37], were also collected. The tower-based albedo measurement scheme follows a strict set of guidelines as established by the International Baseline Surface Radiation Network (BSRN) [38], [39]. BSRN measurement protocols are recognized as the international standard for in situ albedo data, with a review process that includes built-in redundancies and additional quality assurance (QA) checks

TABLE I
GLOBAL STATISTICS (MEAN [COEFFICIENT OF VARIATION %]) FOR CAR
(INCLUDING 30- AND 250-m MODELS), MODIS, AND LANDSAT-TM SPECTRAL BRF VALUES

	Blue	Red	NIR
Landsat-TM	0.0424 [19.81%]	0.0789 [28.77%]	0.2823 [19.09%]
CAR-30m	0.0385 [22.07%]	0.0854 [29.74%]	0.3236 [13.35%]
CAR-250m	0.0377 [19.62%]	0.0892 [23.87%]	0.3292 [11.02%]
MODIS	0.0494 [13.36%]	0.0949 [13.69%]	0.3097 [09.59%]

Coefficient of Variation [CV% = Standard Deviation / Mean]

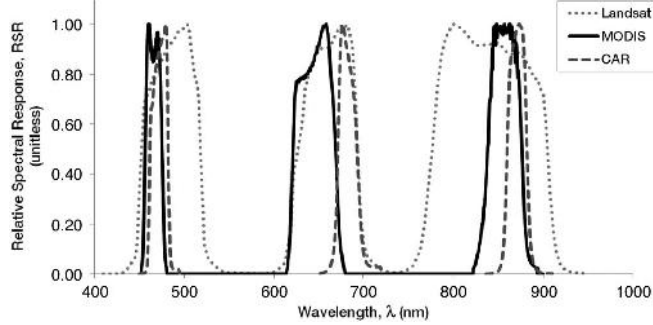


Fig. 3. RSR curves for Landsat-TM (gray dotted lines), MODIS (black solid lines), and CAR (gray dashed lines) in the blue (475 nm), red (662 nm), and NIR (852 nm) regions.

(e.g., standard units, naming conventions, and reporting intervals) to maintain consistency (< 2%) within the larger network-wide BSRN database [40], [53].

B. Spatial Representativeness Analysis

On account of the uncertainties arising from direct comparison between sparsely sampled *in situ* albedo measurements and their corresponding satellite products, an analysis of the representativeness of the surface heterogeneity at the ARM-CART was performed to determine whether direct “point-to-pixel” comparisons were appropriate during the CLASIC’07 observing period. The methodology used here, based on work first described in [7], uses a number of geostatistical attributes derived from semivariograms [41]–[43]. The scheme begins by extracting variogram model parameters (e.g., range, sill, and nugget) from 30 m Landsat-TM albedos to quantify the spatial representativeness of a measurement site. Three spatial elements (1.0 km², 1.5 km², and 2.0 km²) are then selected to better recreate the footprint of satellite observations from different scan angles [9].

Results in Fig. 4, based on the Landsat-TM scene acquired on DOY 154, 2007, show the variogram functions and relevant model parameters for three Landsat-TM subsets derived over the ARM/CART site on 3 June 2007 (DOY 154). The ground diameter footprint as seen by the downward-facing pyranometer atop the ARM/CART site’s tower is shown [Fig. 4(a), white circle]. The footprint of the 60-m radiation is about 750 m in diameter ($FOV = 81^\circ$)

$$f = 2H \tan(FOV^\circ) \quad (4)$$

where f is the circular footprint of ground tower measurements, H [m] is the instrument height, and FOV [degrees] is its field of

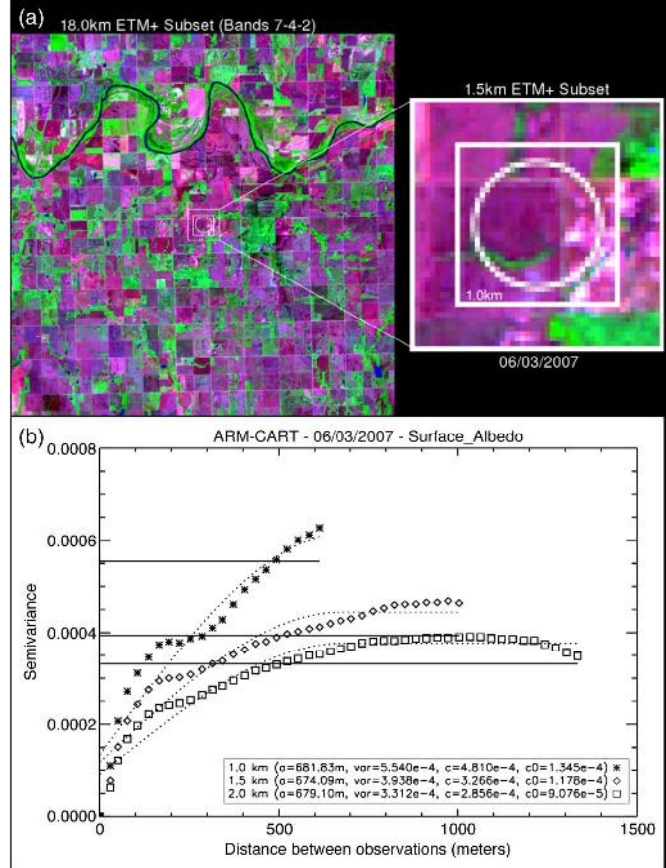


Fig. 4. (a) At-ground shortwave BRF composites (Landsat-TM Bands 7-4-2) centered at the ARM-CART 60-m radiation tower. Pasture fields and trees are in shades of green (both light and dark tones) and purple, crops and bare areas are seen in light-pink, light-lavender, magenta, and pale-pink, and water is seen in dark-blue and black. (b) Variogram estimator (points), spherical model (dotted curves), and sample variance (solid straight lines) obtained over the ARM-CART using surface albedos derived from an ETM+ scene retrieved on 3 June 2007 using regions of 1.0 km (asterisks), 1.5 km (diamonds), and 2.0 km (squares).

view. Throughout the analysis stage in Section IV, a Gaussian filter was applied to the CAR, MODIS, and Landsat-TM data to compute spatially-integrated albedos that represented the tower’s ground-projected instantaneous field of view (GIFOV).

The overall variability of the ARM/CART site, as determined by the sample variances (Fig. 4(b), solid black lines) is larger for the smaller 1.0 km² spatial element (5.540e-04) than for the larger 2.0 km² element (3.938e-04). The variogram estimators for each of the ETM+ subsets [Fig. 4(a), point values] also begin to separate at short distances (< 100 m). When a measurement site is spatially representative, the overall variability between the internal (1.0 km²) components of the measurement

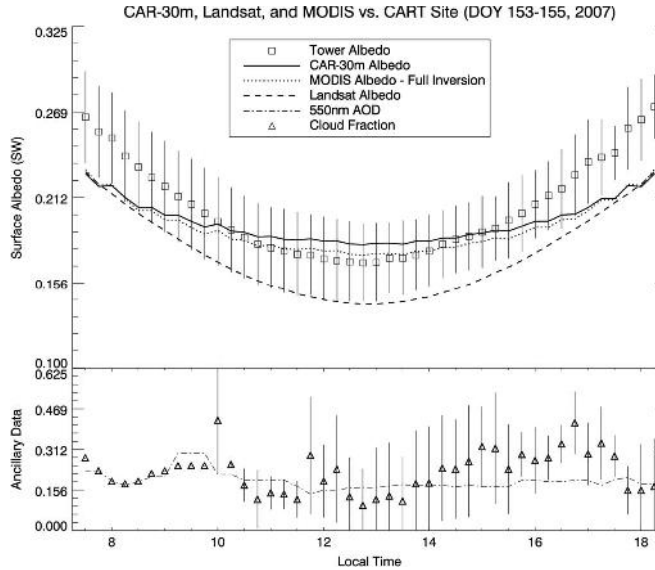


Fig. 5. (Top) Comparisons between instantaneous retrievals of surface albedo (3-day averaged samples in 15-min intervals) derived from CAR-30 m (solid black line), MODIS full inversion retrievals (dotted lines), Landsat-TM (dashed lines), and tower-based measurements (squares with error bars) acquired at the ARM/CART site throughout a 3-day period surrounding the Landsat-TM overpass date (DOY 154, 2007). (Bottom) Coincident retrievals of aerosol optical depth at 550 nm from the local AERONET sun photometer (dashed dotted lines) and cloud fraction estimates (triangles with error bars). Total rainfall for this 3-day period was 0.21 inches.

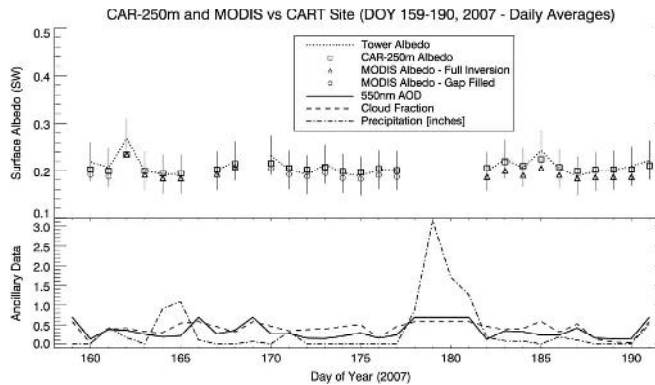


Fig. 6. Comparisons between instantaneous albedos (daily intervals) derived from CAR-250 m and MODIS, and tower-based measurements acquired at the ARM/CART site throughout a 32-day period surrounding CLASIC'07 Flight #1928 (DOY 175, 2007).

site and its adjacent landscape ($1.5\text{--}2.0 \text{ km}^2$) should be similar in magnitude and the variogram estimators for each spatial element should trail each other until they reach the variogram range (a). The spatial trends observed for the ARM/CART site during the period of CLASIC'07 are nonetheless indicative of a measurement site that is internally more heterogeneous than its surrounding area. Furthermore, the scale of the heterogeneity (as defined by the variograms range values, a) is consistently larger ($> 670 \text{ m}$) than the effective MODIS pixel size (500 m); but smaller than the tower albedo meter's GIFOV (750 m). From Fig. 4, one can also see that the footprint of the CART tower is able to capture the full range of surface conditions extending to a 1.0 km^2 region.

In the past, these scaling differences have resulted in errors on the order of a 15% disagreement between the MODIS

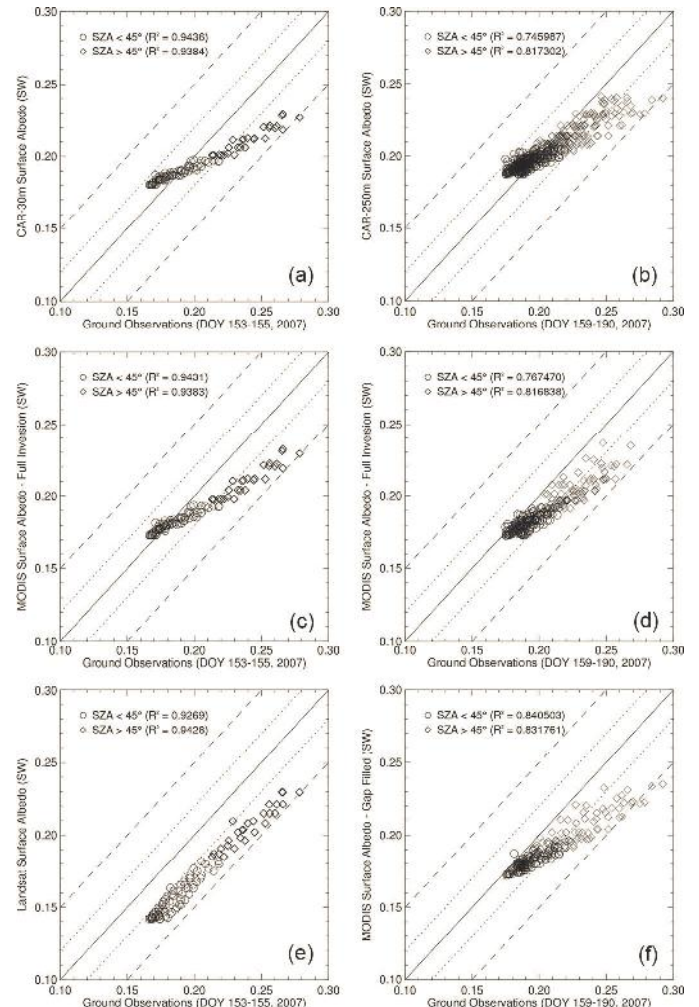


Fig. 7. Scatter plots evaluate the instantaneous albedo reconstructions against tower-based observations at the ARM/CART site for: (a) CAR-30 m during DOY 153–155, (b) CAR-250 m during DOY 159–190, (c) MODIS full inversion results for DOY 153–155, (d) MODIS full inversion results for DOY 159–190, (e) Landsat-TM albedos for DOY 153–155, and (f) MODIS gap-filled results for DOY 159–190. The solid line is the one-to-one line and the dashed lines are ± 0.02 and ± 0.05 units. The statistical results (R^2 -square) are displayed for two solar zenith angle (SZA) ranges: SZA < 45° (circles) and SZA > 45° (diamonds).

and field-measured values [4]–[6], [8], [9]; although to our knowledge, a reliable quantification of the resulting scaling uncertainty has not been performed. Thus, to better characterize and reduce the propagation of measurement error when evaluating the MODIS data at the individual pixel level, spatially-distributed albedos acquired at fine spatial resolutions are necessary (cf., Section IV).

C. Comparisons to Tower-Based Measurements

Following the albedo reconstruction periods described in Fig. 1, results in Figs. 5–7 show comparisons between the tower-based estimates against CAR, MODIS, and Landsat-TM. The error bars tracking the tower-based estimates in Figs. 5 and 6 illustrate the estimated range of uncertainty resulting from spatial scaling effects ($\pm 15\%$ minus the standard deviation in tower albedo for a given time interval, cf., Section III-B).

TABLE II
ACCURACY^a (GROUND-RETRIEVAL) AND UNCERTAINTY^b (RMS OF ABSOLUTE ERROR OR RMSE) RESULTING FROM COMPARISONS BETWEEN TOWER-BASED (CART SITE), AIRBORNE (CAR-30 m), AND SATELLITE-DERIVED (MODIS AND LANDSAT-TM) ALBEDOS AS ILLUSTRATED IN FIG. 5. THE TOTAL SAMPLE SIZES (n) FOR TWO SOLAR ZENITH ANGLE (SZA) RANGES ARE SHOWN

DOY 153–155,2007	SZA < 45° (n = 73)			SZA > 45° (n = 27)		
	CAR-30m	MODIS	Landsat-TM	CAR-30m	MODIS	Landsat-TM
Accuracy (Bias)	-0.0033	0.0025	0.0290	0.0294	0.0303	0.0356
Uncertainty (RMSE)	0.0096	0.0086	0.0295	0.0310	0.0314	0.0362

^aAccuracy = arithmetic mean (Tower - Sensor)

^bUncertainty: RMS of absolute error = $\sqrt{\text{arithmeticmean}(\text{Tower} - \text{Sensor})^2}$

TABLE III
ACCURACY AND UNCERTAINTY VALUES RESULTING FROM A 32-DAY COMPARISON BETWEEN GROUND-BASED (CART), AIRBORNE (CAR-250 m), AND SATELLITE-DERIVED (MODIS) ALBEDOS AS ILLUSTRATED IN FIG. 6. SETUP IS THE SAME AS TABLE II

DOY 159–190,2007	SZA < 45°			SZA > 45°		
	CAR-250m (n = 289)	MODIS Full Inversion (n=129)	MODIS Gap Filled (n=160)	CAR-250m (n = 159)	MODIS Full Inversion (n=63)	MODIS Gap Filled (n=96)
Accuracy (Bias)	-0.0042	0.0090	0.0112	0.0121	0.0234	0.0282
Uncertainty (RMSE)	0.0082	0.0107	0.0130	0.0173	0.0253	0.0314

Measurements of ancillary parameters (e.g., aerosol optical depth (AOD) at 550 nm, cloud fraction, and daily precipitation estimates) are also reported. A series of scatter plots were produced to evaluate the albedo reconstructions for all clear-sky observations (15-min intervals with cloud fraction < 0.6) over the two periods of interest: DOY 153–155 [Fig. 7(a)–(c)] and DOY 159–190 [Fig. 7(d)–(f)]. The statistical results (R-square) are displayed for two solar zenith angle (SZA) ranges (SZA < 45° and 70° > SZA > 45°). Additional statistical results for the mean absolute error (i.e., Tower—Sensor) and RMSE values are shown in Tables II and III.

Results in Fig. 5 show the usual “U-shaped” diurnal trend in instantaneous albedo that reaches a minimum value around local solar noon time. The cloud fraction estimates in Fig. 5 reveal larger and more recurring instances of cloud-contamination in the late morning and afternoon periods. The time series plot in Fig. 6 illustrates the effect that precipitation patterns can have on the MODIS BRDF retrieval and the downstream daily albedo reconstructions. These extended rainfall periods resulted in gaps in the daily averaged albedo values (particularly for DOY 178–181) in addition to a number of MODIS BRDF retrieval periods to rely on the gap-filled retrieval method (i.e., DOY 160–161 and DOY 170–177). Since the CAR BRDF retrievals were based on a very stable time period (rainfall had paused for 6 consecutive dates centered on DOY 175), the albedo reconstructions were not as sensitive to landscape-level changes in precipitation. Visual assessments of the ARM/CART site during CLASIC’07 also confirm that the area covering the tower-based footprint was comprised of well drained crops and soils that were less prone to forming patches of standing water. As a result, the CAR albedos were consistent with the tower observations (albeit for a period of ±16 days surrounding DOY 175).

The CAR and MODIS albedos met the accuracy requirements established for the high quality MODIS operational albedos at 500 m (the greater of 0.02 units or ±10% of surface measured values) [45]. Results were more accurate at SZA < 45°, with MODIS and CAR values staying well within ±5% of tower-based estimates (cf., Fig. 7). For the DOY 159–190 retrieval period (Table III), the accuracy of CAR was slightly higher than MODIS by 1.07% (at SZA < 45°) and 3.42% (at 70° > SZA > 45°). For the DOY 153–155 measurement period (Table II), MODIS was slightly more accurate than CAR at SZA < 45° (by 0.43%); while the opposite was found at 70° > SZA > 45° (0.17%). The accuracy results for the MODIS full inversion retrievals were slightly more robust than their gap-filled counterparts by 0.0023 (or 0.98% relative) at SZA < 45° and by 0.0061 (or 2.61% relative) at 70° > SZA > 45°.

Correlations between Landsat-TM albedos and the tower-based measurements were high (R-squares = 0.92–0.94); but the SW retrievals were influenced by a negative bias on the order of 0.030 (or 12% relative). Measurement differences may have risen in the retrieved Landsat-TM BRF values themselves; as they were likely impacted by the rainfall patterns that preceded the Landsat-TM overpass (DOY 154). However, our results confirm only minor reductions in the mean absolute bias (from 0.0323 to 0.0318, for all SZAs) when constraining the observations to the Landsat-TM date of acquisition (DOY 154).

IV. REGIONAL ASSESSMENT

In the previous section, CAR retrievals were shown to be of sufficient accuracy and consistency to reproduce the diurnal variations in albedo across the ARM/CART site throughout the entire period of CLASIC’07. Using the CAR-30 m and CAR-250 m instantaneous albedos as “ground-truth”, we now

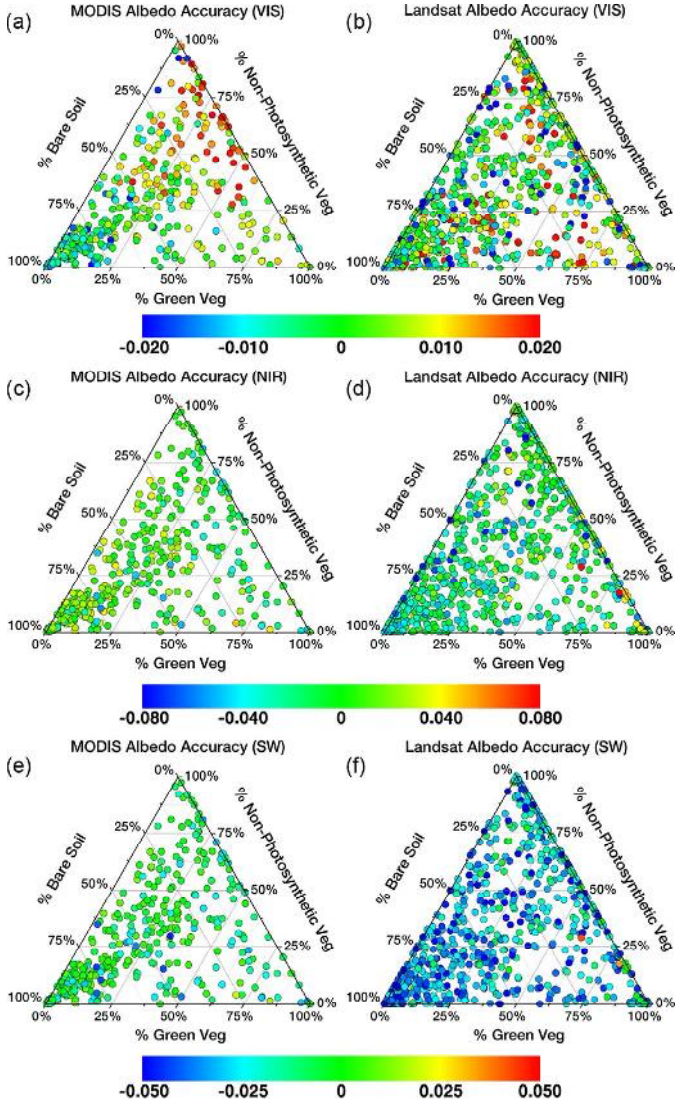


Fig. 8. Ternary diagrams illustrating the pixel-specific accuracy of instantaneous albedos (Satellite—CAR) at Visible (a)–(b), NIR (c)–(d), and SW (e)–(f) broadband channels for a $10 \text{ km} \times 10 \text{ km}$ region centered on the ARM/CART site. The sample size is 368 for (MODIS) and 820 for Landsat-TM. The absolute limit for each color bar corresponds to relative error bounds of $\pm 20\%$.

employ standard error propagation techniques [44] to quantify the pixel-specific accuracy of MODIS and Landsat-TM retrievals over a mixture of landscapes extending beyond the tower observation footprint at the ARM/CART site. Specifically, CAR albedo reconstructions were matched to the scale of MODIS and Landsat-TM to minimize spatial scaling and pixel georegistration errors. Additional checks were also performed to limit the sampling of CAR and MODIS pixels to the highest quality “majority” full BRDF inversion values. For CLASIC’07 Flight #1928, this resulted in 368 samples obtained at the MODIS scale and 820 samples at the aggregated Landsat scale; each of which was evaluated following the same albedo reconstruction periods presented in Section III (Fig. 1). Landsat-TM albedos were further aggregated at 240 m grid cells to minimize uncertainties due to scaling effects and georegistration inaccuracies. Fig. 8 illustrates the regional assessment results for MODIS and Landsat-TM focusing on comparisons against CAR-derived albedos over the entire CLASIC’07 study domain

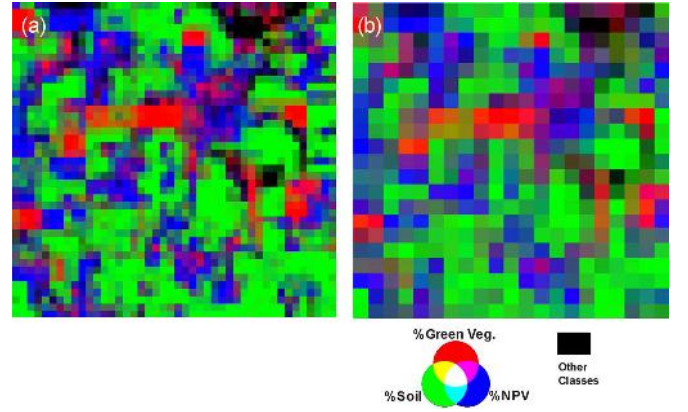


Fig. 9. Fractional cover estimates (%) of green vegetation (e.g., corn/milo, shrubs, and forest), non-photosynthetic vegetation (NPV) (e.g., pasture, wheat/stubble), and bare soils, using (a) 240-m aggregated grid cells for Landsat-TM (left), and (b) 500-m grid cells for MODIS (right).

($10 \text{ km}^2 \times 10 \text{ km}^2$ centered on the ARM/CART site). For this analysis, ternary diagrams were used to help characterize the impact of spatial heterogeneity on the accuracy of the satellite retrievals. Results were expressed in terms of three major fractional cover types: % green vegetation, % non-photosynthetic vegetation (NPV), and % bare soils (cf., Fig. 9). To determine the composition of a point within the triangular area, a series of three lines can be drawn through the point of interest, with each line parallel to a side of the triangle. With these lines in place, the percentage of each fractional cover type can be determined. Thus, points located near the top originate from landscapes dominated by NPV, points located near the bottom-left correspond to areas dominated by bare soils, points located near the bottom-right correspond to areas dominated by green vegetation, and point located near the center of the triangle correspond to spatially heterogeneous landscapes.

Results in Table IV indicate that the majority ($> 50\%$) of MODIS and Landsat-TM broadband albedos were found to be below the $\pm 10\%$ margin of error. For the MODIS VIS broadband, most of the samples that fell above the $\pm 10\%$ error margin experienced positive biases on the order of 0.0155 absolute units; particularly across landscapes with high cover fractions of NPV [Fig. 8(a)].

Both MODIS and Landsat-TM albedos remained stable in the NIR broadband, with $> 80\%$ of samples meeting the 10% accuracy requirement. Results for Landsat-TM were less stable in the SW broadband channel; with negative systematic biases (-0.03) affecting 72% of tested samples. The accuracy results for the Landsat-TM albedos appeared to be independent of fractional cover or structural heterogeneity. This is likely due to the minimum mapping unit for the fractional cover data (30 m); which was too coarse for capturing the scale of the heterogeneity at the Landsat sub-pixel scale. Relative to the previous “point/tower-to-pixel” assessment of MODIS SW albedos (Section III-C), results also indicate a reduction in the mean absolute error of 0.01823 (or 7.8% relative; cf., Table IV). Since the Landsat-TM albedos already contain information at fine spatial resolution, improvements between the tower-based and airborne based accuracy estimates were nominal for all broadband channels ($< 2.5\%$).

TABLE IV

ACCURACY ESTIMATES FOR MODIS AND LANDSAT-TM BROADBAND ALBEDO VALUES ($SZA < 70^\circ$), BASED ON THE RELATIVE NUMBER OF SAMPLES (%) THAT FELL UNDER ERROR BOUNDS OF $\pm 5\%$, $\pm 10\%$, $\pm 20\%$, AND $> 20\%$. THE LAST ROW “ Δ BIAS (ALL OBS.)” SHOWS THE OVERALL IMPROVEMENT IN SATELLITE ALBEDO RETRIEVAL ACCURACY (BASED ON COMPARISONS WITH AIRBORNE CAR ALBEDOS) THAT RESULTED FROM THE REMOVAL OF SUB-GRID SCALE MISMATCH ERRORS BETWEEN THE REMOTELY-SENSED AND GROUND-MEASURED ALBEDO ESTIMATES

Accuracy Bounds	MODIS (n = 368)			Landsat TM (n = 820)		
	VIS	NIR	SW	VIS	NIR	SW
< 5%	36.68%	45.65%	56.52%	39.02%	48.29%	7.56%
< 10 %	69.29%	91.30%	83.97%	67.32%	80.98%	28.05%
< 20%	94.57%	100.00%	99.18%	94.02%	98.54%	87.68%
> 20%	5.43%	0.00%	0.82%	5.98%	1.46%	12.32%
Δ Bias (all obs.)	1.02%	0.39%	7.80%	2.52%	1.87%	1.69%

V. CONCLUSION AND FOLLOW-UP ACTIVITIES

The diurnal performance of the MODIS and Landsat-TM albedo algorithms [10], [18], [45] is evaluated using field and airborne measurements coincident with Landsat-TM and multi-date MODIS Terra/Aqua overpasses. For the broad range of mixed vegetation and structural types examined during the period of CLASIC’07, the overall accuracy of MODIS albedos remained within a $\pm 10\%$ margin of error for all solar zenith angles (SZAs). However, results also reveal a high degree of variability in the visible (0.3–0.7 μm) broadband channels; mostly over areas with fractions of non-photosynthetic vegetation. However, we note that the lack of high-quality “majority” 500 m MODIS BRDF pixels during the entire CLASIC’07 experiment hindered the band-dependent quality controls, as outliers were more difficult to identify. This was particularly the case in the VIS broadband, where cloud contamination and mixed-pixel contamination are highly likely. Despite such limitations, results obtained indicate that MODIS albedos were able to capture spatially heterogeneous landscapes with high accuracy across all broadband channels. These results are consistent with previous comparisons between spectral albedos derived from MODIS and airborne SSFR data [46]; which have shown that both sensors can capture inhomogeneous surface albedo scene changes with accuracies of 6–10% [47]. The results from both our local (tower-based) and regional (airborne-based) assessments further confirm a 7.8% improvement in MODIS SW albedo retrieval accuracy. We assert this improvement resulted from the removal of measurement uncertainties when directly scaling-up the tower albedo results from the ARM/CART site to the MODIS (500 m) satellite footprint. This reduction also corresponds (both in magnitude and spectral dependence) to previous documented errors involving the spatial aggregation of linear BRDF model parameters over the same set of mixed agricultural landscapes [16]. Our results therefore confirm the potential for BRDF scaling errors to propagate to both the downstream surface BRF (reflectance) and albedo retrieval; particularly when cross-comparing results obtained at different spatial scales.

At present, the sources of systematic error in the Landsat-TM SW albedo reconstructions could not be entirely assessed. However, our findings are not inconsistent with previous studies

that have also found negative biases on the order of 0.03 in the SW [10]. Looking at the Landsat albedo processing chain, we note that there are various “upstream” sources of systematic and random errors that could have affected the retrievals (e.g., random errors due to a slight overcorrection in the reflectance retrieval, or small differences in the RSRs). Another consideration is the assumption of spatial/temporal uniformity at the Landsat (30 m) pixel scale. As shown in this study, this will particularly affect retrievals where heterogeneous conditions are being lumped into a single land cover class (e.g., bare soil areas not being properly partitioned into dry, wet, and damp conditions.) As upcoming algorithm refinement efforts are adopted and validated as part of the Landsat albedo processing stream (including adoption of global MODIS Collection V6 daily rolling 500 m albedos), this will allow us to reduce the potential impact of systematic error on the Landsat albedo retrieval.

While recent product development, intercomparison, and validation efforts have focused almost entirely on the retrieval of surface albedos for a single SW broadband value, it is important to note that most numerical prediction models, global climate, and biogeochemical models currently in use call for surface energy fluxes and some biophysical variables to be calculated separately by disentangling broadband albedos into fractional areas of bare soil and vegetation [48]–[51]. It is therefore important to continue examining how the accuracies of global albedo products are holding up in these spectral regimes. Likewise, the uncertainties that may impact satellite-inferred albedo trends must be assessed and expressed in terms of a reference suite of sensors that can overcome the foretold errors due to sub-grid scale mismatch and the effects of land surface heterogeneity. It is thus critical that continuous, long-term tower measurements of surface albedo and radiation fluxes be done in concert with intensive airborne measurement campaigns that can focus on addressing sources of retrieval uncertainties at both plot-level (< 90 m) to landscape-level (> 90 m) scales.

ACKNOWLEDGMENT

The authors thank the CLASIC Science team (B. Schmidt, M. Miller, P. Lamb, J. Ogren, J. Mather *et al.*) and Sky Research, J-31 aircraft team (D. Thrasher, S. Kaiser, K. Zimmerer,

and R. Billings) for their support during the CLASIC experiment; as well as two anonymous reviewers for their valuable comments. The U.S. Department of Agriculture is an equal opportunity provider and employer.

REFERENCES

- [1] A. Cescatti, B. Marcolla, S. K. S. Vannan, J. Y. Pan, M. O. Román, X. Yang, P. Ciais, R. B. Cook, B. E. Law, G. Matteucci, M. Migliavacca, E. Moors, A. D. Richardson, G. Seufert, and C. B. Schaaf, "Intercomparison of MODIS albedo retrievals and in situ measurements across the global FLUXNET network," *Remote Sens. Environ.*, vol. 121, pp. 323–334, Jun. 2012.
- [2] J. T. Morisette, J. L. Privette, and C. O. Justice, "A framework for the validation of MODIS land products," *Remote Sens. Environ.*, vol. 83, no. 1/2, pp. 77–96, Nov. 2002.
- [3] Y. F. Jin, C. B. Schaaf, F. Gao, X. W. Li, A. H. Strahler, W. Lucht, and S. Liang, "Consistency of MODIS surface bidirectional reflectance distribution function and albedo retrievals: 1. Algorithm performance," *J. Geophys. Res.*, vol. 108, no. D5, p. 4158, Mar. 2003.
- [4] Y. F. Jin, C. B. Schaaf, C. E. Woodcock, F. Gao, X. W. Li, A. H. Strahler, W. Lucht, and S. Liang, "Consistency of MODIS surface bidirectional reflectance distribution function and albedo retrievals: 2. Validation," *J. Geophys. Res.*, vol. 108, no. D5, p. 4159, Mar. 2003.
- [5] J. Liu, C. B. Schaaf, A. H. Strahler, Z. Jiao, Y. Shuai, Q. Zhang, M. Román, J. A. Augustine, and E. G. Dutton, "Validation of Moderate Resolution Imaging Spectroradiometer (MODIS) albedo retrieval algorithm: Dependence of albedo on solar zenith angle," *J. Geophys. Res.-Atmospheres*, vol. 114, no. D1, p. D01106, Jan. 2009.
- [6] M. O. Román, C. B. Schaaf, P. Lewis, F. Gao, G. P. Anderson, J. L. Privette, A. H. Strahler, C. E. Woodcock, and M. Barnsley, "Assessing the coupling between surface albedo derived from MODIS and the fraction of diffuse skylight over spatially-characterized landscapes," *Remote Sens. Environ.*, vol. 114, no. 4, pp. 738–760, Apr. 2010.
- [7] M. O. Román, C. B. Schaaf, X. Yang, C. E. Woodcock, A. H. Strahler, R. H. Braswell, P. S. Curtis, K. J. Davis, D. Dragoni, M. L. Goulden, L. Gu, D. Y. Hollinger, T. E. Kolb, T. P. Meyers, J. W. Munger, J. L. Privette, A. D. Richardson, T. B. Wilson, and S. C. Wofsy, "The MODIS (collection V005) BRDF/albedo product: Assessment of spatial representativeness over forested landscapes," *Remote Sens. Environ.*, vol. 113, no. 11, pp. 2476–2498, Nov. 2009.
- [8] J. G. Salomon, C. B. Schaaf, A. H. Strahler, F. Gao, and Y. F. Jin, "Validation of the MODIS bidirectional reflectance distribution function and albedo retrievals using combined observations from the Aqua and Terra platforms," *IEEE Trans. Geosci. Remote Sens.*, vol. 44, no. 6, pp. 1555–1565, Jun. 2006.
- [9] Z. Wang, C. B. Schaaf, A. H. Strahler, J. Wang, C. E. Woodcock, M. J. Chopping, M. O. Román, A. V. Rocha, and Y. Shuai, "Evaluation of Moderate-resolution Imaging Spectroradiometer (MODIS) snow albedo product (MCD43A) over tundra," *Remote Sens. Environ.*, vol. 117, pp. 264–280, Feb. 2012.
- [10] Y. Shuai, J. Masek, F. Gao, and C. B. Schaaf, "An algorithm for the retrieval of 30-m snow-free albedo from Landsat surface reflectance and MODIS BRDF," *Remote Sens. Environ.*, vol. 115, no. 9, pp. 2204–2216, Sep. 2011.
- [11] J. A. Augustine, G. B. Hodges, C. R. Cornwall, J. J. Michalsky, and C. I. Medina, "An update on SURFRAD—The GCOS surface radiation budget network for the continental United States," *J. Atmos. Ocean. Technol.*, vol. 22, no. 10, pp. 1460–1472, Oct. 2005.
- [12] J. Susaki, Y. Yasuoka, K. Kajiwara, Y. Honda, and K. Hara, "Validation of MODIS albedo products of paddy fields in Japan," *IEEE Trans. Geosci. Remote Sens.*, vol. 45, no. 1, pp. 206–217, Jan. 2007.
- [13] R. Bindlish, T. Jackson, R. Sun, M. Cosh, S. Yueh, and S. Dinardo, "Combined passive and active microwave observations of soil moisture during CLASIC," *IEEE Geosci. Remote Sens. Lett.*, vol. 6, no. 4, pp. 644–648, Oct. 2009.
- [14] G. C. Heathman, M. Larose, M. H. Cosh, and R. Bindlish, "Surface and profile soil moisture spatio-temporal analysis during an excessive rainfall period in the Southern Great Plains, USA," *CATENA*, vol. 78, no. 2, pp. 159–169, Aug. 2009.
- [15] S. A. McFarlane, K. L. Gaustad, E. J. Mlawer, C. N. Long, and J. Delamere, "Development of a high spectral resolution surface albedo product for the ARM Southern Great Plains central facility," *Atmos. Meas. Tech.*, vol. 4, no. 9, pp. 1713–1733, Sep. 2011.
- [16] M. O. Román, C. K. Gatebe, R. Poudyal, C. B. Schaaf, Z. Wang, and M. D. King, "Variability in surface BRDF at different spatial scales (30 m–500 m) over a mixed agricultural landscape as retrieved from airborne and satellite spectral measurements," *Remote Sens. Environ.*, vol. 115, no. 9, pp. 2184–2203, Sep. 2011.
- [17] S. Y. Kotchenova, E. F. Vermote, R. Matarrese, and F. J. Klemm, "Validation of a vector version of the 6 S radiative transfer code for atmospheric correction of satellite data. Part I: Path radiance," *Appl. Opt.*, vol. 45, no. 26, pp. 6726–6774, Sep. 2006.
- [18] C. B. Schaaf, F. Gao, A. H. Strahler, W. Lucht, X. Li, T. Tsang, N. C. Strugnell, X. Zhang, Y. Jina, J.-P. Muller, P. Lewis, M. Barnsley, P. Hobson, M. Disney, G. Roberts, M. Dunderdale, C. Doll, R. P. d'Entremont, B. Hu, S. Liang, J. L. Privette, and D. Roy, "First operational BRDF, albedo and nadir reflectance products from MODIS," *Remote Sens. Environ.*, vol. 83, no. 1/2, pp. 135–148, Nov. 2002.
- [19] C. K. Gatebe, M. D. King, S. Platnick, G. T. Arnold, E. F. Vermote, and B. Schmid, "Airborne spectral measurements of surface-atmosphere anisotropy for several surfaces and ecosystems over southern Africa," *J. Geophys. Res.*, vol. 108, no. D13, p. 8489, Jul. 2003.
- [20] M. D. King, M. G. Strange, P. Leone, and L. R. Blaine, "Multiwavelength scanning radiometer for airborne measurements of scattered radiation within clouds," *J. Atmos. Ocean. Technol.*, vol. 3, no. 3, pp. 513–522, Sep. 1986.
- [21] W. Lucht, C. B. Schaaf, and A. H. Strahler, "An algorithm for the retrieval of albedo from space using semi-empirical BRDF models," *IEEE Trans. Geosci. Remote Sens.*, vol. 38, no. 2, pp. 977–998, Mar. 2000.
- [22] W. Wanner, X. Li, and A. H. Strahler, "On the derivation of Kernels for Kernel-driven models of bidirectional reflectance," *J. Geophys. Res.*, vol. 100, no. D10, pp. 21077–21089, Jan. 1995.
- [23] W. Wanner, A. H. Strahler, B. Hu, P. Lewis, J. Muller, X. Li, C. L. Barker, M. Schaaf, and J. Barnsley, "Global retrieval of bidirectional reflectance and albedo over land from EOS MODIS and MISR data: Theory and algorithm," *J. Geophys. Res.*, vol. 102, no. D14, pp. 17143–17161, Jan. 1997.
- [24] J. Martonchik, C. Bruegge, and A. H. Strahler, "A review of reflectance nomenclature used in remote sensing," *Remote Sens. Rev.*, vol. 19, no. 1–4, pp. 9–20, Dec. 2000.
- [25] G. Schaepman-Strub, M. E. Schaepman, T. H. Painter, S. Dangel, and J. V. Martonchik, "Reflectance quantities in optical remote sensing—definitions and case studies," *Remote Sens. Environ.*, vol. 103, no. 1, pp. 27–42, Jul. 2006.
- [26] P. Lewis and M. Barnsley, "Influence of the sky radiance distribution on various formulations of the Earth surface Albedo," in *Proc. Colloq. Int. Mes. Phys. Sign. Teledetect.*, Val d'Isere, France, 1994, pp. 707–716.
- [27] J. J. Butler and C. A. Barnes, "The use of transfer radiometers in validating the visible to shortwave infrared calibrations of radiance sources used by instruments in NASA's Earth observing system," *Metrologia*, vol. 40, no. 1, pp. S70–S77, Feb. 2003.
- [28] C. K. Gatebe, J. J. Butler, J. W. Cooper, M. Kowalewski, and M. D. King, "Characterization of errors in the use of integrating-sphere systems in the calibration of scanning radiometers," *Appl. Opt.*, vol. 46, no. 31, pp. 7640–7651, Nov. 2007.
- [29] A. Trishenko, Y. Luo, M. Cribb, and K. Hamm, "Surface spectral albedo intensive operational period at the ARM SGP site in August 2002: Results, analysis, and future plans," in *Proc. 13th ARM Sci. Team Meeting*, 2004, pp. 1–8.
- [30] S. Liang, A. H. Strahler, and C. Walther, "Retrieval of land surface albedo from satellite observations: A simulation study," *J. Appl. Meteorol.*, vol. 38, no. 6, pp. 712–725, Jun. 1999.
- [31] A. Berk, T. W. Cooley, G. P. Anderson, P. K. Acharya, L. S. Bernstein, L. Muratov, J. Lee, M. Fox, S. M. Adler-Golden, J. H. Chetwynd, M. L. Hoke, R. B. Lockwood, J. A. Gardner, C. C. Borel, and P. E. Lewis, "MODTRAN5: A reformulated atmospheric band model with auxiliary species and practical multiple scattering options, sensors, systems, and next-generation satellites," in *Proc. SPIE*, 2004, pp. 78–85.
- [32] A. H. Strahler, W. Lucht, C. B. Schaaf, T. Tsang, F. Gao, X. Li, J.-P. Muller, P. Lewis, and M. J. Barnsley, "MODIS BRDF/Albedo Product: Algorithm Theoretical Basis Document Version 5.0..," Washington, DC, USA, NASA EOS-MODIS 1999, 1999.
- [33] Q. Zhang, "A Global Spatially and Temporally Complete Reflectance Anisotropy Database to Improve Surface Characterization for Albedo Modeling," Ph.D. dissertation, Dept. of Geogr. and Environ., Boston Univ., Boston, MA, USA, 2008.
- [34] P. Lewis, "The utility of kernel-driven BRDF models in global BRDF and albedo studies," in *Proc. IGARSS*, Florence, Italy, 1995, pp. 1186–1188.

- [35] K. D. Knobelpiesse, B. Cairns, B. Schmid, M. Román, and C. B. Schaaf, "Surface BRDF estimation from an aircraft compared to MODIS and ground estimates at the Southern Great Plains site," *J. Geophys. Res.-Atmospheres*, vol. 113, no. D20, p. D20105, Oct. 2008.
- [36] N. A. Streck, D. Rundquist, and J. Connors, "Spectral signature of selected soils," *Rev. Brasil. Agrometeorol., Santa Maria*, vol. 11, no. 1, p. 184, Dec. 2003.
- [37] B. N. Holben, D. Tanre, A. Smirnov, T. F. Eck, I. Slutsker, N. Abuhassan, W. W. Newcomb, J. S. Schafer, B. Chatenet, F. Lavenu, Y. J. Kaufman, J. Vande Castle, A. Setzer, B. Markham, D. Clark, R. Frouin, R. Halthore, A. Karniel, N. T. O'Neill, C. Pietras, R. T. Pinker, K. Voss, and G. Zibordi, "An emerging ground-based aerosol climatology: Aerosol optical depth from AERONET," *J. Geophys. Res.*, vol. 106, no. D11, pp. 12067–12097, Jan. 2001.
- [38] L. B. J. McArthur, "Baseline Surface Radiation Network (BSRN) Operations Manual V2.1," World Climate Research Program, Geneva, Switzerland, WCRP 121, WMO/TD-No. 1274, Apr. 2005. [Online]. Available: http://www.wmo.ch/pages/prog/wcrp/PG_Reports_WCRPSeries.html
- [39] WMO, "World Meteorological Organization Commission for Instruments and Methods of Observation (WMO/CIMO) Guide to Meteorological Instruments and Methods of Observation," Preliminary Seventh Edition, Geneva, Switzerland, Report WMO-No. 8, 2006. [Online]. Available: http://www.wmo.int/pages/prog/gcos/documents/gruanmanuals/CIMO/CIMO_Guide-7th_Edition-2008.pdf
- [40] C. B. Schaaf, J. Cihlar, A. Belward, E. Dutton, and M. Verstraete, "Albedo and Reflectance Anisotropy, ECV-T8: Assessment of the Status of the Development of Standards for the Terrestrial Essential Climate Variables," FAO, Rome, Italy, 2009.
- [41] S. S. Carroll and N. Cressie, "A comparison of geostatistical methodologies used to estimate snow water equivalent," *Water Resources Bull.*, vol. 32, no. 2, pp. 267–278, Apr. 1996.
- [42] J. C. Davis, *Statistics and Data Analysis in Geology*, 2nd ed. New York, NY, USA: Wiley, 1986.
- [43] E. H. Isaaks and R. M. Srivastava, *An Introduction to Applied Geostatistics*. New York, NY, USA: Oxford Univ. Press, 1989.
- [44] G. B. M. Heuvelink, *Error Propagation in Environmental Modeling With GIS*. Boca Raton, FL, USA: CRC Press, 1998.
- [45] C. B. Schaaf, J. Martonchik, B. Pinty, Y. Govaerts, F. Gao, A. Lattanzio, J. Liu, A. Strahler, and M. Taberner, "Retrieval of surface albedo from satellite sensors," in *Advances in Land Remote Sensing: System, Modeling, Inversion and Application*, S. Liang, Ed. New York, NY, USA: Springer-Verlag, 2008, pp. 219–243.
- [46] P. Pilewskie, J. Pommier, R. Bergstrom, W. Gore, S. Howard, M. Rabbette, B. Schmid, P. V. Hobbs, and S. C. Tsay, "Solar spectral radiative forcing during the Southern African regional science initiative," *J. Geophys. Res.*, vol. 103, no. D13, p. 8486, 2003.
- [47] O. Coddington, K. S. Schmidt, P. Pilewskie, W. J. Gore, R. W. Bergstrom, M. O. Román, J. Redemann, P. B. Russell, J. Liu, and C. C. Schaaf, "Aircraft measurements of spectral surface albedo and its consistency with ground-based and space-borne observations," *J. Geophys. Res.*, vol. 113, no. D17, p. D17209, Sep. 2008.
- [48] M. B. Ek, K. E. Mitchell, Y. Lin, E. Rogers, P. Grunmann, V. Koren, G. Gayno, and J. D. Tarpley, "Implementation of the upgraded Noah land surface model in the National Centers for Environmental Prediction operational mesoscale Eta model," *J. Geophys. Res.*, vol. 108, no. D22, p. 8851, Nov. 2003.
- [49] T. A. T. Kaptué, J.-L. Roujeau, and S. Faroux, "ECOCLIMAP-II: An ecosystem classification and land surface parameter database of western Africa at 1 km resolution for the Africa Monsoon Multidisciplinary Analysis (AMMA) project," *Remote Sens. Environ.*, vol. 114, no. 5, pp. 961–976, May 2010.
- [50] R. D. Koster, M. J. Suarez, A. Ducharne, M. Stiegler, and P. Kumar, "A catchment-based approach to modeling land surface processes in a general circulation model 1. Model structure," *J. Geophys. Res.*, vol. 105, no. D20, pp. 24809–24822, Jan. 2000.
- [51] J. Noilhan and J.-F. Mahfouf, "The ISBA land surface parametrization scheme," *Global Planetary Change*, vol. 13, no. 1–4, pp. 145–159, Jun. 1996.
- [52] J. G. Masek, E. F. Vermote, N. Saleous, R. E. Wolfe, F. G. Hall, F. K. Huemmrich *et al.*, "A Landsat surface reflectance data set for North America, 1990–2000," *Geosci. Remote Sens. Lett.*, vol. 3, pp. 68–72, 2006.
- [53] J. A. Augustine and E. G. Dutton, "Variability of the surface radiation budget over United States from 1996 through 2011 from high-quality measurements," *J. Geophys. Res.*, 2012, doi: 10.1029/2012JD018551.



Miguel O. Román (M'00) received the B.Sc. degree in electrical engineering from the University of Puerto Rico, Mayagüez Campus, Mayaguez, Puerto Rico and M.Eng. degree in systems engineering from Cornell University, Ithaca, NY USA, in 2004 and 2005, respectively, and his Ph.D. degree in remote sensing from Boston University, Boston, MA, USA, in 2009.

He is a member of Land Product Evaluation and Test Element (PEATE) team; part of NASA's Science Data Segment's effort to evaluate the operational Land algorithms that are being used for the Visible Infrared Imager Radiometer Suite (VIIRS) onboard the Suomi National Polar-Orbiting Partnership (NPP) satellite. Through his participation in several field campaign programs (FLUXNET, NACP, ARM-DoE, and BSRN) and intense observing periods (e.g., Cheas'06, CLASIC'07, ARCTAS'08, ECO-3D'11). He has used *in situ*, airborne, and satellite data to understand the role of reflectance anisotropy (BRDF), scale, and spatial heterogeneity in the retrieval of terrestrial essential climate variables; especially under conditions of seasonal and rapid surface change. His research and technical efforts as the Land scientist for NASA's Cloud Absorption Radiometer (CAR) and the BRDF, Albedo, Clouds and Aerosols Radiometer (BACAR) have led to new approaches for global inter-comparison of moderate-resolution land science products and the development of new algorithms for studying ecosystem change. He has also taken the lead for the NASA Land Science community in developing plans and achieving consensus in the areas of global product validation and approaches for producing environmental data records to meet the needs of both the operational (NOAA) and science research (NASA) communities.

Dr. Román is the recipient of several prestigious awards including the NASA Early Career Achievement Medal and the IEEE Geoscience and Remote Sensing Society (GRSS) Gold Early Career Award.



Charles K. Gatebe received the B.Sc. degree in meteorology, mathematics, & physics and M.Sc. degree in meteorology degrees from the University of Nairobi, Nairobi, Kenya, in 1990 and 1994, respectively, and the Ph.D. degree in atmospheric sciences from the University of the Witwatersrand, South Africa, in 1999.

He taught courses on air pollution using nuclear related techniques at the Institute of Nuclear Science, University of Nairobi from 1995–1998 and came to NASA Goddard Space Flight Center (GSFC) in 1999 as a Resident Research Associate of the Universities Space Research Association (USRA). He was an associate research scientist with the University of Maryland Baltimore County (2000–2011), and currently, he is a Senior Research Scientist with USRA based at GSFC. Dr. Gatebe is the recipient of World Meteorological Organization Young Scientist award in 2000, and several NASA meritorious awards. He's the principal investigator of NASA's Cloud Absorption Radiometer (CAR).



Yanmin Shuai received the Ph.D. degree in geography and in remote sensing from Beijing Normal University, Beijing, China, and Boston University, Boston, MA, respectively, in 2008 and 2009, with support from the joint doctoral program between Beijing Normal University and Boston University.

After graduation, she became a Research Scientist at the Earth Resources Technology Inc. working on NASA GSFC projects. Her research interests are focused on the development of routine direct broadcast anisotropic and radiative products for MODIS as well as approaches for Landsat albedo, the detection and monitoring of phenological events over agriculture and forested regions, and the radiative evolution of terrestrial ecosystems disturbed by fires, harvesting, and insect epidemics.



Zhuosen Wang received his B.S. degree in Geography from Beijing Normal University, Beijing, China and Ph.D. degree in geography from Boston University in 2003 and 2011, respectively. He has been a Research Fellow in the Environment, Earth, and Ocean Sciences Department at the University of Massachusetts, Boston, MA, USA.

His areas of interest include the modeling and evaluation of the anisotropic characteristics and albedo of the land surface during the snow covered and dormant period, the monitoring of the vegetation phenology using satellite data and the carbon cycle using a regional land surface model in coastal areas.



Tao He received the B.E. degree in photogrammetry and remote sensing from Wuhan University, China, and the Ph.D. degree in geography from the University of Maryland, College Park, MD, in 2006 and 2012, respectively.

He has been a Research Associate in the Department of Geographical Sciences at the University of Maryland, College Park. His areas of interest include surface anisotropy and albedo modeling, data fusion of satellite products, and long-term regional and global surface radiation budget analysis.



Feng Gao received the B.A. degree in geology and the M.E. degree in remote sensing from Zhejiang University, Hangzhou, China, in 1989 and 1992, respectively, the Ph.D. degree in geography from Beijing Normal University, Beijing, China, in 1998, and the M.S. degree in computer science from Boston University, Boston, MA, USA, in 2003.

From 1992 to 1998, he was a Research Assistant at the Nanjing Institute of Geography and Limnology, Chinese Academy of Science, Nanjing, China. From 1998 to 2004, he was a Research Associate Professor

at the Department of Geography and a Researcher in the Center for Remote Sensing, Boston University. From 2004 to 2011, he was a Research Scientist with Earth Resources Technology, Inc. and the NASA Goddard Space Flight Center. Since 2011, he has been a Research Scientist with the Hydrology and Remote Sensing Laboratory, USDA Agricultural Research Service. His recent research interests include remote sensing modeling, multi-sensor data fusion, and vegetation biophysical parameter retrieving for crop and ecosystem condition monitoring. He has been a member of Landsat Science Team since 2006.



Shunlin Liang (M'94–SM'01) received the Ph.D. degree from Boston University, Boston, MA, USA.

He is currently a Professor with the department of geographical sciences, University of Maryland, College Park, MD, USA, and the college of global change and earth system sciences, Beijing Normal University, Beijing, China. His main research interests focus on estimation of land surface variables from satellite data, earth energy balance, and assessment of environmental impacts of vegetation changes. He published about 160 peer-reviewed journal

papers, authored the book *Quantitative Remote Sensing of Land Surfaces*, edited the book *Advances in Land Remote Sensing: System, Modeling, Inversion and Application*, and co-edited the book *Advanced Remote Sensing: Terrestrial Information Extraction and Applications*.

Dr. Liang is an Associate Editor of the IEEE TRANSACTION ON GEOSCIENCE AND REMOTE SENSING and also a guest editor of several remote sensing related journals.



Crystal B. Schaaf (M'92) received the S.B. and S.M. degrees in meteorology from the Massachusetts Institute of Technology, Cambridge, MA, USA, in 1982, the M.L.A. degree in archaeology from Harvard University, Cambridge, MA, USA, in 1988, and the Ph.D. degree in geography from Boston University, Boston, MA, USA, in 1994.

She is a Science Team member working on the development of operational products from NASA's MODerate Resolution Imaging Spectrometer (MODIS) to monitor the Earth's environments

from the Terra and Aqua polar-orbiting space platforms. She is also a science team member for the Landsat-8 satellite program and for the VIIRS (Visible Infrared Imaging Radiometer Suite) sensor on board the Suomi National Polar-orbiting Partnership (NPP). Currently, she is a Professor in the Environmental, Earth and Ocean Sciences Department at the University of Massachusetts, Boston. Her early research focused the use of remote sensing in automated cloud analyses and the detection of initiating convective clouds. Her current interests include modeling reflectance anisotropy and albedo and using remote sensing data to reconstruct and monitor the reflectance characteristics of various land surfaces, including vegetation phenology and land surface change. More recently, she has also been involved in the development and use of ground-based lidar systems to characterize biomass and vegetation structure.

Jeffrey G. Masek received the B.A. degree in geology from Haverford College in 1989, and the Ph.D. degree in geological sciences from Cornell University in 1994.

He is a Research Scientist in the Biospheric Sciences Branch at the NASA Goddard Space Flight Center. His research interests include mapping land-cover change in temperate environments, application of advanced computing to remote sensing, and satellite remote sensing techniques. Dr. Masek has held previous positions at the University of Maryland, Hughes Information Systems, and Cornell University. At the University of Maryland, he acted as project manager for the REALM Image Database system, which pioneered automated, large-area land-cover analyses through parallel processing of Landsat data, and was also Deputy Team Leader for the Landsat Science Team. At Hughes Information System, he managed the collaborative prototyping program for the EOSDIS Core System (ECS) project, which sought out and funded innovative earth science information prototypes from the academic community.